Available online at www.sciencedirect.com
ScienceDirect
International Journal of Mass Spectrometry 265 (2007) 159–168
International Journal of Mass Spectrometry
www.elsevier.com/locate/ijms

Comparative gas-phase activation of two similar non-covalent heptameric protein complexes: gp31 and GroES

Rimco B.J. Geels [a,c], Saskia M. van der Vies [b], Albert J.R. Heck [c], Ron M.A. Heeren [a,c,*]

[a] *FOM Institute for Atomic and Molecular Physics, Kruislaan 407, 1098 SJ Amsterdam, The Netherlands*
[b] *Department of Biochemistry and Molecular Biology, Vrije Universiteit, De Boelelaan 1083, 1081 HV Amsterdam, The Netherlands*
[c] *Department of Biomolecular Mass Spectrometry, Utrecht University, Sorbonnelaan 16, 3584 CA Utrecht, The Netherlands*

Received 4 November 2006; received in revised form 30 January 2007; accepted 7 February 2007
Available online 14 February 2007

Abstract

Using electrospray ionisation, non-covalently bound protein complexes can be transferred intact into the gas-phase and analysed and manipulated in a mass spectrometer. Here, two large (70–80 kDa) similar non-covalent protein complexes, gp31 and GroES, both cochaperonin to GroEL in *Escherichia coli*, were manipulated and compared inside a mass spectrometer using several gas-phase activation techniques. Nozzle-skimmer dissociation and collision-activated dissociation were performed using a quadrupole time-of-flight mass spectrometer and a Fourier transform ion cyclotron resonance mass spectrometer. Dissociation of these heptameric complexes mainly results in hexamers and monomers. There are no significant differences in gas-phase stability between the two complexes, but their fragmentation pathways exhibit considerable differences. Charge division over the fragments and overall charge losses during dissociation of the complexes differ clearly between GroES and gp31. These effects also differ between the various activation techniques, demonstrating that the different activation techniques yield complementary data. Combined, the different activation techniques are used to elucidate the dissociation mechanism and the degree of unfolding of the ejected monomer from the complex. The different behaviour of the two protein complexes is rationalized to be dependent on the gas-phase structures of gp31, GroES and their fragmentation products.

Keywords: Non-covalent complex; Ion activation; SORI-CAD; CAD; FTICRMS

1. Introduction

Electrospray ionisation (ESI) can be used to transfer non-covalently bound complexes into the gas-phase for intact protein complex analysis in a mass spectrometer. ESI is a soft ionisation method that retains labile quaternary associations of protein complexes [1–3]. Very small complexes, such as protein ligand interactions, up to intact ribosomes have been examined with ESI [4–6]. The structure and gas-phase stability of these complexes can be examined by means of ion activation techniques. By trapping the intact complexes in a Fourier transform-ion cyclotron resonance-mass spectrometer (FT-ICR-MS), the complexes can be examined and manipulated for extended periods of time. This creates possibilities for ion activation via infrared multi-photon dissociation (IRMPD), surface induced dissociation (SID), electron capture dissociation (ECD), blackbody infrared radiative dissociation and sustained off-resonance irradiation collision activated dissociation (SORI-CAD) or on-resonance CAD [7–9]. Non-covalent protein complexes of increasingly larger masses are subject to structural analysis by mass spectrometry [10,11]. Activation and dissociation analysis of over 50 kDa complexes is now routinely done. In this paper, we report on two non-covalent complexes, GroES and gp31, which have been subjected to gas-phase stability experiments.

Both gp31 and GroES are cochaperonin of the GroEL protein in *Escherichia coli*. In *E. coli* many proteins need the GroEL-GroES chaperonin machinery to be able to fold into their biologically active native state [12]. GroEL functions as the folding cage, the so-called Anfinsen cage [13], and GroES is the lid of this cage The chaperonin complex is involved in the folding of approximately 15% of all the *E. coli* proteins [14]. These proteins vary greatly in size and function, illustrating the

* Corresponding author at: FOM Institute for Atomic and Molecular Physics, Kruislaan 407, 1098 SJ Amsterdam, The Netherlands. Tel.: +31 206081234; fax: +31 206684106.
E-mail address: heeren@amolf.nl (R.M.A. Heeren).

1387-3806/$ – see front matter © 2007 Elsevier B.V. All rights reserved.
doi:10.1016/j.ijms.2007.02.008

versatility of this chaperonin complex. This broad functionality of the complex is the main reason why it is being studied very extensively [15–19].

E. coli can get infected by Bacteriophage T4. As part of the reproduction of the bacteriophage, its major capsid protein, gp23, needs to fold into its native state. To achieve the native state, the chaperonin machinery of the *E. coli* cannot be used, i.e., gp23 cannot fold with the help of the normal GroEL-GroES complex. The GroES lid of the folding cage has to be substituted by the bacteriophage-encoded protein gp31 [20]. Gp31 shows structural similarity to GroES. Both are non-covalent complexes of seven identical subunits arranged in a circular fashion, exhibiting seven-fold symmetry. The gp31 heptamer is slightly heavier (84 kDa) than groEL (73 kDa).

The origin of this functional difference has been investigated extensively [21,22]. It is believed that the difference in function arises from a difference in structure between the two protein complexes [23]. The size of the folding cage for the GroEL-gp31 complex is somewhat larger than that of the GroEL-GroES complex. This enlargement allows for the accommodation of the relatively large gp23 (56 kDa), which is close to the upper size limit of proteins that can be accommodated by GroEL-GroES chaperonin and will probably not fit into this folding cage [21]. The crystal structures of the two proteins are reproduced in Fig. 1. Besides the increase in cavity size, there are other structural differences visible between GroES and gp31. Gp31 has a large mobile loop that might have other functions than just assisting in the size increment of the folding cage. In addition the roof loop that is present in GroES is missing in gp31, which might allow the formation of a larger folding cage.

Using native mass spectrometry of non-covalent complexes [24], possible with FT-ICR-MS and quadrupole time-of-flight (q-ToF) mass spectrometry, it is possible to uncover additional differences between the two complexes. For instance, differences in the stability and structure of the complexes in the gas-phase can become apparent when activating these molecules in the mass spectrometer. In this paper, we report on the analysis of both complexes in the gas-phase using nozzle-skimmer dissociation, on-resonance CAD and SORI-CAD. These techniques are all based on collisional activation, but the activation and analyses timescales of the experiments vary. These techniques will render complementary information on collisional activation of the protein complexes.

2. Experiment

Both co-chaperonins, gp31 and GroES were over-expressed in *E. coli* strain MC1009 [25] and purified as described previously [26–28]. The proteins were buffer exchanged to a 1 mM ammonium acetate buffer, pH 6.8, by using ultra filtration filters with a cut-off of 5000 Da (Millipore, Bedford). Final concentrations of gp31 and GroES in the spray sample were 13.5 and 28 μM, respectively. Protein concentrations are given based on the gp31 and GroES monomer. Denatured solutions of gp31 and GroES consist of 14 μM protein dissolved in a buffer of water (29%), methanol (69%) and acetic acid (2%).

The experiments were performed using a modified Bruker APEX 7.0e FT-ICR-MS equipped with an infinity cell [29]. Experimental control hard- and software were developed in-house and have been described elsewhere [29]. Elevated pressure

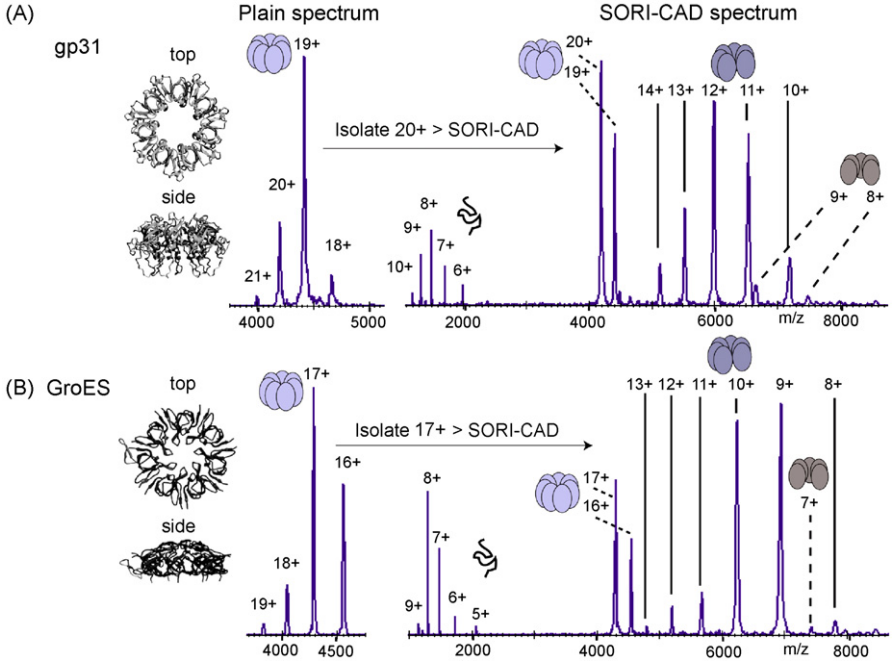

Fig. 1. (A) Plain spectrum obtained for the gp31 non-covalent heptamer on the left side, flanked by the crystal structure [23], revealing the seven-fold symmetry of the protein complex. The result of isolation of the 20+ charge state and subsequent SORI-CAD is shown on the right-hand side of the top graph. Visible are the remaining parent, a charge stripped heptamer, fragment hexamers and pentamers at the high-mass end and at the low-mass end highly charged, unfolded monomers. (B) Plain spectrum obtained for the GroES non-covalent heptamer. Here, the 17+ charge state is isolated and collision-activated. The cartoons next to the peaks in the spectra indicate the stoichiometry of the various species.

in the source octopole (∼2 mbar) facilitated transfer of the large intact protein complexes into the gas-phase and to the ICR cell [30]. Ions were accumulated inside the ICR cell using gas-assisted trapping with typical accumulation times of 10–12 s. Individual charge states of the protein heptamers were isolated using SWIFT pulses [31].

Nozzle-Skimmer (NS-) dissociation was performed by scanning the capillary voltage from 0 to 300 V while keeping the skimmer voltage constant at 25 V. The dissociation is thus actually "capillary-skimmer dissociation", but it is comparable to what is commonly called NS-dissociation in orthogonal-acceleration time-of-flight mass spectrometry. We will use NS-CAD to refer to this technique. Ions are accelerated out of the capillary-skimmer region where they collide with neutral air molecules. The pressure in this region is in on the order of 10^{-2} mbar. The activated ions and their dissociation products are subsequently transported to the ICR-cell and analysed.

CAD and SORI-CAD experiments were also performed. In CAD, the SWIFT isolated charge states were excited on-resonance for increasing amounts of time, where after the activated ions collide with neutral argon gas. In SORI-CAD, the ions were excited off-resonance to produce ions with varying kinetic energy [32]. SORI-CAD was performed with a +1000 Hz offset and argon collision gas, using procedures described previously [33]. SORI-CAD is a slow-heating technique that only activates the lowest energy decay channel, whereas on-resonance CAD activates the ions in a much shorter time period. On-resonance CAD is usually thought not to be able to add enough internal energy to large ions/ion complexes to allow fragmentation. Longer excitation via SORI-CAD is necessary to achieve the threshold activation energy for dissociation. As it turns out, both techniques deliver enough energy to dissociate the complex and the results of both techniques can be compared.

CAD was also performed using a q-ToF I instrument from Micromass. This mass spectrometer is adapted for tandem mass spectrometry on macromolecular protein complexes [34]. The source pressure was elevated to 8 mbar to cool the ions and facilitate ion transfer into the gas-phase [35–37]. Selected parent charge state ions were accelerated into the collision quadrupole and the resulting fragments analysed with the ToF system. Results of all the activation techniques were compared.

The timescales with respect to activation and analyses times for the various techniques differ. For the various (on-resonance) CAD experiments, the activation of the protein complexes is fast, via several energetic collisions, whereas the activation with SORI-CAD proceeds slower, via multiple low-energy collisions. After activation, the analysis times also differ between the q-ToF and the FT-ICR-MS. The time-of-flight measurement of the activation products proceeds within milliseconds, whereas analysis in the FT-ICR-MS takes several seconds.

3. Results

In Fig. 1, on the left-hand-side, the plain mass spectra for gp31 and GroES are shown, together with their crystal structures. The solution phase K_d of GroES is estimated to be 1×10^{-38} M^6 [38]. For the molarities used in these experiments, the equilibrium is almost completely to the heptameric form. For gp31 no measurement of the solution phase dissociation constant exists, but considering the similarity between the two complexes it can be expected that the equilibrium for gp31 will also be shifted to the heptameric complex. Gel filtration experiments confirm that at concentrations between 10 and 25 μM gp31 is in its heptameric form (unpublished data). The gas-phase data confirm that the equilibrium is completely towards the heptameric form, showing only the heptamer stoichiometry in the plain mass spectra.

On the right-hand side of Fig. 1, typical SORI-CAD breakdown diagrams of one specific charge state are shown. Gp31 and GroES exhibit similar behavior upon activation. Activation of the parent ion leads to charge reduction of the parent peak as is visible in the spectrum where the heptamer peak has one less charge. Most likely this lost charge is a charged adduct like sodium or ammonium, present in the solution. It is unlikely that protons are knocked of the complex. The resolution of the spectra is not sufficient to determine the nature of the lost charge carrier. While other groups have reported the loss of a negative charge upon activation of large complexes [39,40], in the experiments in this paper loss of a negative charge has not occurred. Besides charge reduction, the parent heptamer can also fragment upon activation. Fragmentation proceeds via ejection of a subunit from the complex, leaving behind a hexamer. The ejected monomer carries away a disproportionally large share of the total number of charges. This disparate charge distribution has been observed numerous times in CAD experiments of protein complexes [2,11,41–45]. It is believed that Coulombic forces drive the dissociation, which proceeds via the partial unfolding of a single subunit from the complex. While this subunit unfolds, a charge redistribution takes place. When the monomer is sufficiently unfolded and charged, Coulombic repulsion is thought to lead to expulsion of the highly charged monomer. The unfolded monomers appear at the low mass/charge region of the spectrum. The pentamers present in the spectrum can originate via ejection of a dimer from the complex or via subsequent ejection of two monomers. Although dimers are not visible in the spectra, it cannot be concluded that dimmer ejection has not occurred, because the dimers probably fall apart into two monomers after ejection.

CAD experiments of the proteins on the FT-ICR-MS and the q-ToF I also resulted in both charge reduction of the parent species and dissociation of the complex into hexamers and highly charged monomers mostly.

4. Thermodynamic stabilities of GroES and gp31 are comparable

Comparison of the thermodynamic stabilities of the two complexes was done via collision activation experiments on the q-ToF I. For gp31 individual charge states were isolated in separate experiments (19+ up to 22+) and subject to CAD. The same was done for various charge states of GroES (18+ up to 20+). The survival yields of the parent ions were calculated for all collision energies used in the experiment. The survival yield was calculated by dividing the ion count of the remaining parent after activation by the total ion count of the remaining parent

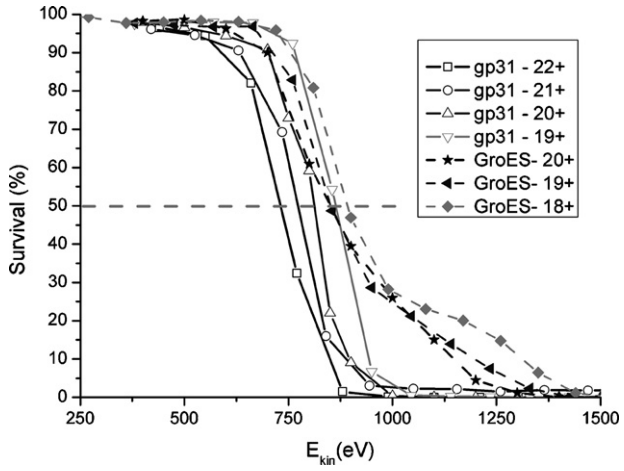

Fig. 2. Breakdown diagrams constructed for the various parent charge states of gp31 and GroES. The breakdown diagrams are constructed by calculating the survival percentage of heptamer compared to all activation products present. The survival percentages are shown as a function of kinetic energy with which the parent enters the collision cell. The 50% survival yield points show a trend to lower kinetic energies for higher charge states, compensating for less Coulombic repulsion within the complex for lower charge states. The differences in 50% survival yield points between the two species can be explained by this charge-effect and do not indicate any intrinsic thermodynamic stability difference between the two proteins in the gas-phase.

plus fragment species. The constructed survival yield diagrams for all parent charge states are shown in Fig. 2. The collision voltages (V_{coll}) are scaled with the charges (q) of the various parent ions to obtain the kinetic energy ($E_{kin,lab}$) with which the ions enter the collision cell ($E_{kin,lab} = q \times V_{coll}$). As is immediately evident from this figure, with increasing charge state the gas-phase complexes are thermodynamically less stable. Less kinetic energy is needed to achieve 50% survival yield for the higher charged ions. This 50% survival yield point is indicative for the mean of the initial internal energy distribution prior to dissociation [46,47]. Assuming that the number of degrees of freedom, temperature and the molecular weight of the two complexes are very similar, the difference in location of the 50% inflection points can be considered to be indicative for the relative gas-phase thermodynamic stability. Evaluating the observed difference in thermodynamic stability of GroES and gp31, the data show that for the same parent charge state, the 50% survival yields are comparable within error. Any apparent difference in stability is caused by different number of charges on the protein complexes in the gas-phase. The total interaction strength between the subunits for GroES and gp31 is thus comparable, demonstrating that the difference in function of the two complexes in vivo cannot be directly related to differences in their gas-phase thermodynamic stability.

5. The different activation mechanisms result in comparable breakdown diagrams

The q-ToF collisional activation measurements are compared with survival yield curves constructed from activation measurements using on-resonance CAD, SORI-CAD and NS-CAD on the FT-ICR-MS. In Fig. 3A, the gp31 20+ charge state is visualised and in Fig. 3B the 19+ GroES charge state survival yield curves are shown. The 19+ and 20+ charge states are chosen, because they lie closest to the average parent heptamer charge in the NS-CAD experiment. To be able to compare the survival yields of the parent ions for the various experiments in one graph, scaling factors for the degree of activation are needed. Throughout the rest of the paper, in the graphs the 50% survival yield points using the various activation methods will be aligned. The alignment procedure is done via Eqs. (1a) and (1b), creating a new dimensionless quantity: I_{act}, the activation intensity,

$$I_{act} = \frac{E_{kin,lab}}{C_{50}} \quad \text{NS-CAD, q-ToF-CAD and FTMS-CAD} \tag{1a}$$

$$I_{act} = \frac{N_{SORI}\langle E_{kin,lab}\rangle}{C_{50}} \quad \text{FTMS SORI-CAD} \tag{1b}$$

Here, $E_{kin,lab}$ is the resulting laboratory frame kinetic energy of the parent after activation (for NS-CAD the "average" parent), $\langle E_{kin,lab}\rangle$ the average laboratory frame kinetic energy during

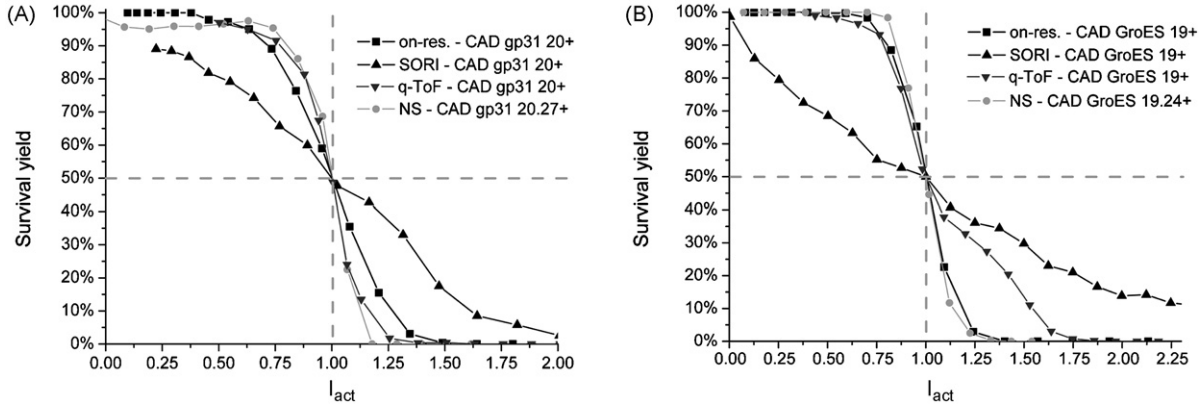

Fig. 3. (A) CAD of the gp31 20+ heptamer for the various activation methods indicated. For NS-Activation, it is not possible to isolate a charge state beforehand. The average charge state of the heptamers at 0 V NS-Activation is 20.27. This is closest to the 20+ charge state for the other activation experiments. The spectra have been linearly aligned at zero activation and 50% survival yield. (B) CAD of the GroES 19+ heptamer. The average parent heptamer charge state at 0 V NS-Activation of GroES is: 19.24. This is compared to the 19+ charge states in the other activation experiments.

Table 1
Overview of the C_{50}-scaling values (in eV) used in Eqs. (1a) and (1b) to align the 50% survival yield points in Figs. 3, 5 and 6 of this paper

C_{50}-values	Gp31				GroES				
	22+	21+	20+	19+	20+	19+	18+	17+	16+
NS-CAD			3,700				3,675		
q-ToF-CAD	730	778	796	864	830	870	929		
on-res. CAD		1,466	1,090	1,205		950	1,130	1,175	1,950
SORI -CAD		17,463	17,603	19,210		19,210	26,963	17,463	30,037

SORI activation, N_{SORI} the total number of SORI cycles and C_{50} is the scaling factor aligning the 50% survival yield points. The C_{50} values for all experiments are given in Table 1. Comparing the kinetic energies needed to achieve 50% survival yield for the on-resonance CAD experiment in the FT-ICR-MS with that needed for the CAD experiment in the q-ToF, somewhat higher kinetic energy is needed in the FT-ICR-MS for both protein complexes. First, ions in the q-ToF were internally hotter than in the FT-ICR-MS before activation, resulting in higher kinetic energy needed for dissociation in the FT-ICR-MS [48]. Second, collision gas pressure used in the FT-ICR-MS was lower than in the q-ToF, resulting in a slower kinetic energy to internal energy conversion resulting in a greater InfraRed (IR) loss. Both factors contribute to the higher kinetic energy needed for dissociation in the FT-ICR-MS. Concerning IR-losses, due to the slow-heating process of SORI-CAD, the effect of IR-loss during activation with this technique becomes considerable and is clearly visible in the decreased slope of the breakdown diagrams. For the q-ToF CAD, FT-ICR-MS on-resonance CAD and NS-CAD the survival yield diagrams have comparable shapes.

These figures also do not reveal any significant difference in gas-phase thermodynamic behavior of the two complexes. In the following paragraphs, however, we will show that, despite the comparable stability of the two protein species using the different activation techniques, there are major differences between techniques and species concerning dissociation mechanics.

6. Dissociation pathways for GroES and gp31 exhibit differences

Activation of the non-covalently bound protein complexes resulted in fragment species with two distinct characteristics: stoichiometry and charge. The experimental results do not indicate that the stoichiometries of the fragment species differ, but the distributions of charges over the various fragments for the different activation techniques show that the dissociation mechanisms of the two complexes differ. The stoichiometric fragmentation pathway of the two complexes, is reproduced in Fig. 4A. This figure shows the parent heptamer dissociating into a hexamer and a monomer. The hexamer has relatively low charge and the (partially) unfolded monomer has relatively high charge. In the next sections, the average charge states of the hexameric and monomeric fragments, resulting from dissociation as in Fig. 4A, will be further analysed.

6.1. Charge state of ejected monomer depends on activation technique, parent charge and parent species

As stated earlier, it is commonly believed that the ejection of the monomer from the complex proceeds via Coulomb-induced unfolding of the monomer and corresponding migration of charge carriers onto the unfolding monomer. Table 2 shows the average charge of the ejected monomers at 50% survival yield for all experiments and species together. It also shows the average charge of monomers present in a mass spectrum of denatured gp31 and GroES. The average charge state is calculated by weighing the charge states in the spectra with their intensities. The charge state of the denatured form of the proteins is considerably higher than those of the ejected monomers during activation. Since we are assuming Coulomb-induced unfolding, this means the Coulomb repulsion is not further reduced by migrating more charges onto the monomer (considering the fact that the supply of charges is limited by the parent charge) and consequently the monomer is less unfolded as compared to the denatured protein. During dissociation, the charges are located at the sites with the highest gas-phase basicity. Table 2 also reveals the variation of the monomer charge with the different parent

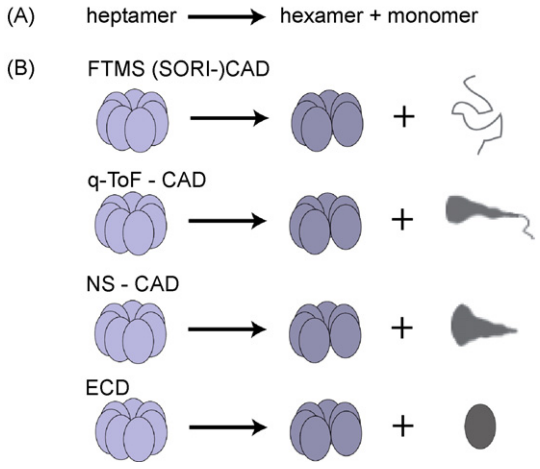

Fig. 4. (A) The major dissociation pathway for both the GroES heptamer and the gp31 heptamer. This pathway holds for all examined charge states and activation mechanisms. It indicates dissociation of the non-covalent parent heptamer into a hexamer and a monomer. The hexamer has a relatively low charge and the monomer has a relatively high charge. This picture is incomplete. Our measurements reveal the effect the activation technique has on the charge states of the fragmentation products. (B) A more detailed representation of the fragmentation products after dissociation. The various activation techniques result in different degrees of unfolding and charging of the monomer.

Table 2
Overview of average monomer charge states

Species	Parent charge	q-ToF	FT-ICR-MS		
		CAD	on-res. CAD	SORI-CAD	NS-CAD
gp31 monomer	22	7.3	–	–	6.0
	21	7.7	7.9	8.1	
	20	7.4	8.1	8.4	
	19	7.3	8.1	8.3	
	Denatured		11.2		
GroES monomer	20	6.9	–	–	5.0
	19	7.3	8.2	7.9	
	18	7.3	7.8	7.9	
	17	–	7.4	7.4	
	16	–	7.0	7.0	
	Denatured		9.9		

The table shows the average monomer charges at 50% survival yield for the various collisional activation techniques, as well as the average charge of the monomers in the mass spectrum of the denatured protein. All indicated charge states have an error of ±0.2.

protein species and charges and with the activation technique chosen.

6.2. Charge state of the ejected monomer relates to the extent of unfolding

In Fig. 5, for the gp31 21+ parent and the 19+ parent for GroES, the average charges of the monomer and hexamer fragments are shown, along with their combined charge as a function of increasing activation. The other investigated parent charge states (19+ and 20+ gp31 and 18+ GroES) exhibit similar behavior and are not reproduced in this figure. The on-resonance CAD experiments using the FTMS and the CAD experiments using the q-ToF show comparable evolution of the combined charge of the fragment hexamer and monomer, whereby the combined charge is somewhat lower for the q-ToF CAD than for the FTMS on-resonance CAD. Interestingly, the charges are differently distributed over the hexamer and monomer. In the q-ToF CAD experiment, the monomer takes away fewer charges than in the FTMS on-resonance CAD experiment. Since the monomer charge states differ, this suggests that the degree of unfolding of the monomer is different for both experiments because otherwise the charge migration onto the monomer would have been the same. The time frame of activation and the total analysis time is shorter for the q-ToF than for the FTMS; which is also indicated by the higher kinetic energy needed for dissociation in the FT-ICR-MS. The data indicates that the monomer is already ejected from the complex in the q-ToF experiment before the Coulomb-induced unfolding has reached the same degree of unfolding as with the FTMS on-resonance CAD experiment.

Around the 50% survival yield point, there is only a slight difference in monomer charge between on-resonance CAD and SORI-CAD on the FTMS. The q-ToF CAD experiment has slightly lower charged monomers, for most parent charge states; see also Table 2. Despite the fact that SORI-CAD slowly heats the protein complex and thus probably would also allow for more extensive unfolding of the monomer, the monomer charge is not higher than for the FTMS on-resonance CAD experiment. This means the Coulomb-induced unfolding has reached equilibrium

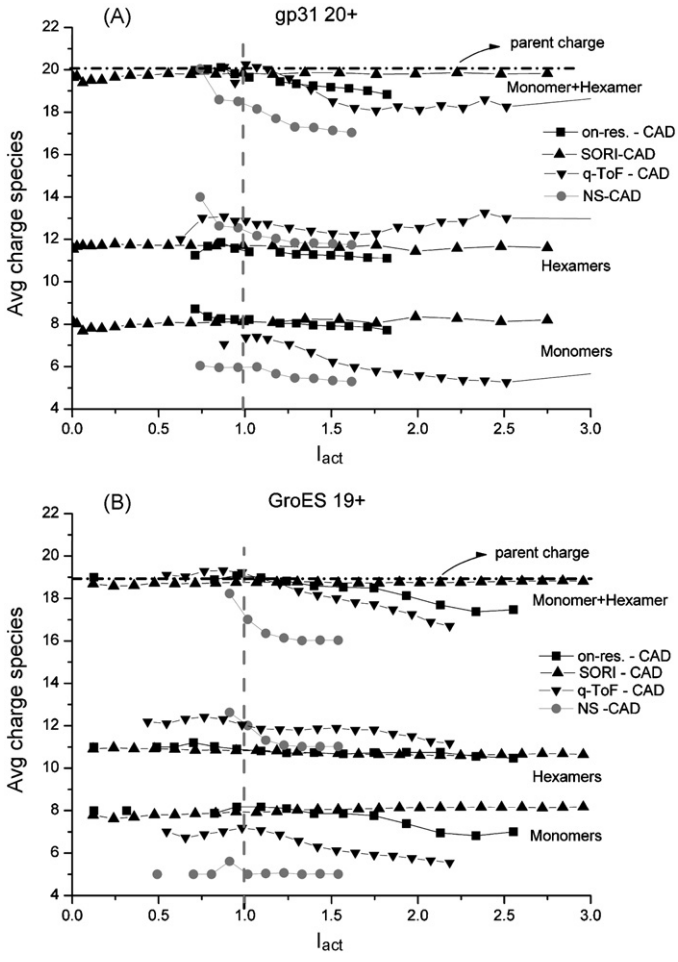

Fig. 5. Evolution of the average charge of the dissociation products, monomers and hexamers, with increasing activation of the parent heptamer, for the gp31 20+ parent charge state (A) and the GroES 19+ parent charge state (B). The parent charge states not shown exhibit similar behaviour. All activation techniques are shown in one graph. For NS-CAD, the average parent charge state is 20.27 for gp31 and 19.24 for GroES. The 50% survival yield point is indicated by the vertical dashed bar in each graph. Also the combined charges of the monomer + hexamer are shown in the figure, to visualise the overall charge loss with increasing activation.

Table 3
Overview of average hexamer charge states

Species	Parent charge	q-ToF	FT-ICR-MS		
		CAD	on-res. CAD	SORI-CAD	NS-CAD
gp31 hexamer	22	14.6	–	–	12.5
	21	13.8	12.0	12.2	
	20	12.9	11.6	11.5	
	19	12.1	10.8	10.6	
GroES hexamer	20	13.0	–	–	12.0
	19	11.9	10.9	10.8	
	18	11.2	10.2	10.1	
	17	–	9.7	9.6	
	16	–	9.0	9.1	

The table shows the average hexamer charges at 50% survival yield for the various collisional activation techniques. All indicated charge states have an error of ±0.2.

before dissociation occurred. The ejected monomer charge can therefore be seen as an indicator of the degree of unfolding of the monomer.

In an earlier study, we observed no charge redistribution to the ejected monomer in ECD experiments, while a monomer was also ejected from the gp31 protein complex [49]. This was attributed to the shorter time-scale of dissociation for the ECD experiment compared to the (SORI-)CAD experiment. This observation agrees well with the differences in activation time and resulting charge redistribution that we observe in the experiments discussed in this paper. Overall, our findings show that changing the mechanism of activation can influence the degree of unfolding of the ejected monomer.

Fig. 4B shows a schematic representation of these effects. Going from no charge carrier rearrangement ("no" unfolding) to some charge rearrangement ("some" unfolding) to even more charge migration to the monomer ("more" unfolding), by using ECD, NS-CAD, q-ToF CAD and FTMS on-resonance CAD and FTMS SORI-CAD, respectively.

6.3. Activation of complexes results in overall charge loss

In Table 3, the average charges of the remaining hexamers are given. Since the average monomer charge and the average hexamer charge do not add up to the parent charge, charge is somehow lost in the process. Table 4 show these charge deficits from the various measurements. For GroES there is only a small charge deficit present for the 19+ parent at the 50% survival yield point in the FTMS SORI-CAD experiment. For gp31 charge deficits are present in the FTMS experiments for the higher charged parents and seem to increase with increased charge state.

Table 4 also shows that for the q-ToF CAD experiment there is no charge loss at the 50% survival yield point. The average charge states for the q-ToF experiments from Tables 2 to 4 together show that charging of the monomer is restricted by the degree of unfolding of the monomer during dissociation using CAD in the q-ToF. In Table 2, all monomers arising from differently charged parents are approximately equally charged. This means the extra charge with increasing parent charge is not redistributed to the ejecting monomer. Monomer charges when using FTMS on-resonance CAD and SORI-CAD are, however, higher, indicating that in this case the monomer is unfolded more extensively.

6.4. Loss of charge happens during or after dissociation of the complex

Since the experiments also showed charge stripping without dissociation upon activation (see Fig. 1) it is presumable that at least part of the charge loss of the fragments has already occurred

Table 4
Overview of the charge deficits

Species	Parent charge	q-ToF	FT-ICR-MS		
		CAD	on-res. CAD	SORI-CAD	NS-CAD
gp31 charge deficit	22	0.1	–	–	1.8
	21	−0.5	1.1	0.7	
	20	−0.3	0.3	0.2	
	19	−0.4	0.1	0.1	
GroES charge deficit	20	0.1	–	–	2.2
	19	−0.2	−0.1	0.2	
	18	−0.5	0.0	0.0	
	17	–	−0.1	0.0	
	16	–	0.0	−0.1	

The charge deficits are the differences between the average monomer charge + average hexamer charge and the parent heptamer charge. It is calculated for each activation method and charge state. All indicated charge deficits have an error of ±0.3.

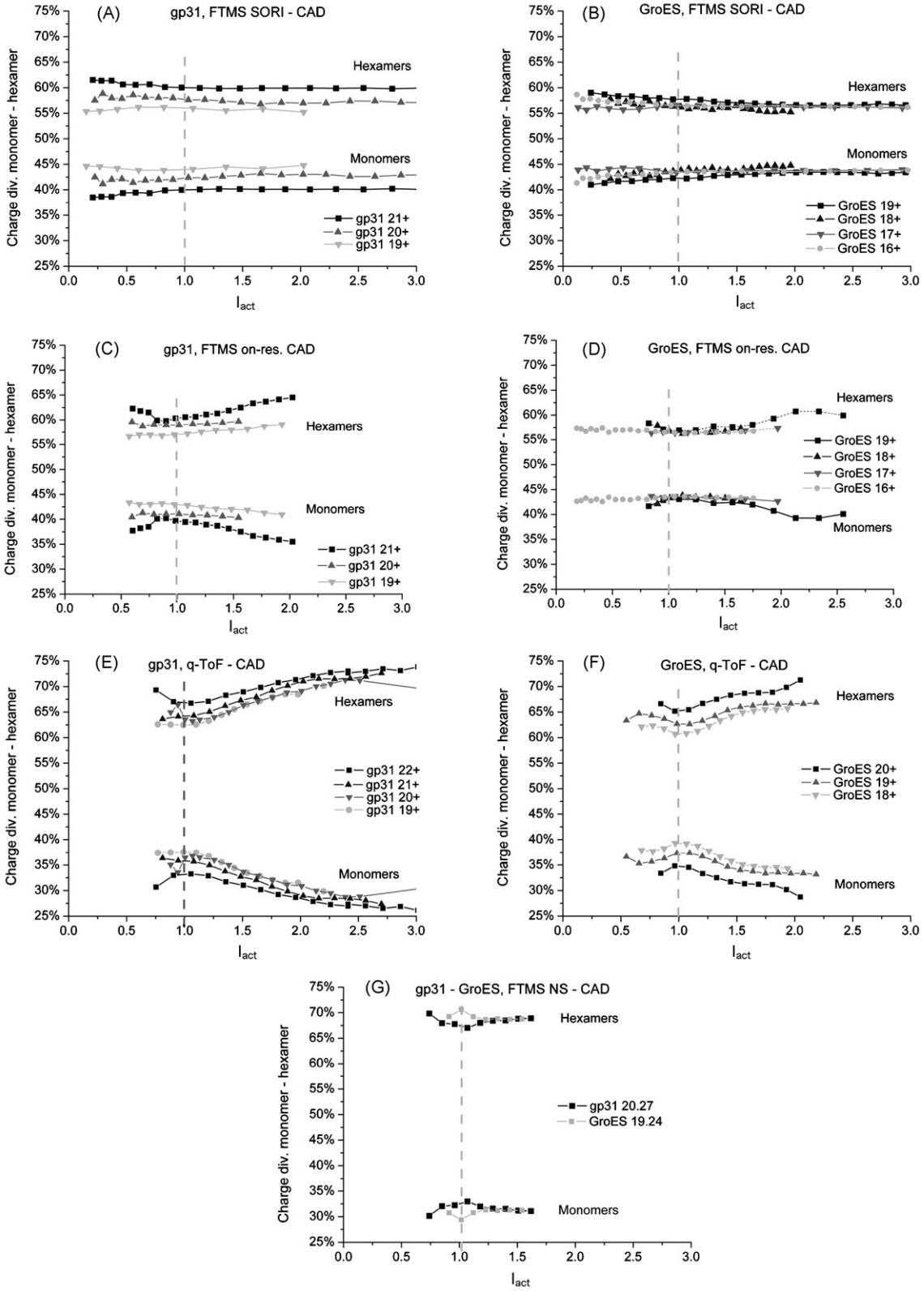

Fig. 6. Evolution of the charge division over the dissociation products, monomers and hexamers, with increasing activation of the parent heptamer. Per species and activation technique all charge states are shown in one graph. The graphs are aligned using Eqs. (1a) and (1b). The 50% survival yield point is indicated by the vertical dashed bar in each graph. The bottom graph combines the results of NS-CAD for both proteins.

well before the onset of dissociation. This is actually not the case, because we observe no difference in dissociation pathway between a charge stripped parent and a parent with fewer charges by itself. For instance, the 21+ gp31 parent with a charge deficit of 2 would be indistinguishable from the 19+ parent without a charge deficit. From Fig. 6, it becomes clear that dissociation of these two parents does not yield the same fragment species in the presented experiments. In this figure, the charge division between the monomers and hexamers is shown with increasing activation for all activation techniques. In Fig. 6C, it can be seen that dissociation of the gp31 21+ parent never yielded the same distribution of charges over the fragments as dissociation of the 20+ and 19+ parents. With increasing activation for the (on-resonance) CAD experiments, the charge loss increased, as shown in Fig. 5 by the decreasing combined monomer and hexamer charge. The charge division over the fragments (Fig. 6C) with increasing activation (i.e., increasing charge deficits) actually diverges from a charge division over the fragments measured for the lower charge states. This confirms that charge stripping and subsequent equilibration does not occur before dissociation, implying that the charge stripping cannot be seen separate from the dissociation of the complex.

6.5. Charge stripping is a kinetic effect

Fig. 5 shows that with growing activation in (on-resonance) CAD the combined fragment charge decreases (i.e., an increasing charge deficit), while for the SORI-CAD experiment the combined fragment charge remains approximately constant. In SORI-CAD, the average internal energy is increased with "continuous low kinetic energy and multiple (soft) collisions", not resulting in more charge loss. This is contrary to (on-resonance) CAD, where the kinetic energy at the start of the collision cascade is increased, resulting in harder collisions and more charge loss. This difference indicates that the charge stripping is a kinetic effect. The charge deficit increases with increasing parent charge state for all experiments. This increasing charge loss is largely accounted for by fewer charges on the ejected monomer. This is evident from the observed decrease in monomer charges (Fig. 5) while the hexamer charge remains relatively constant. This becomes even more clear in Fig. 6C, D and E which shows that the relative charge on the hexamers is increasing compared to the monomer charge. NS-CAD has the highest charge deficit, relative to the average parent charge. While the lowest monomer charge states are achieved with NS-CAD, the hexamer charge states remain comparable to the results for the other FTMS experiments (Fig. 5). Despite the fact that NS-CAD exhibits the largest charge losses, the charge loss is more equally divided over the hexamer and monomer fragment than for the other activation mechanisms that show charge losses. This is shown in Fig. 6F, where the charge division between the fragments during NS-CAD only slightly changes with increasing activation, while the charge loss increases with increasing activation (Fig. 5). This does not agree with the diverging charge divisions in Fig. 6C, D and E when charge loss increases. The exact origin of the charge losses with the ejected monomer and, partly, the fragment hexamer thus remains to be determined.

6.6. Difference gp31 and GroES

Besides the effects of different experimental techniques and parent charge states on the charge states of the fragmentation products, the two different protein complexes exhibit different behaviour.

This study shows that using various activation techniques it is possible to induce different effects on the GroES and gp31 proteins. With rapid, energetic activation, as in NS-CAD, the behavior of the proteins complexes is comparable with respect to charge loss and division over the fragments. Going to a relatively more gentle activation mechanism, the q-ToF CAD, GroES starts showing less charge loss than gp31. This trend continues when using FTMS on-resonance CAD, even gentler activation. When using SORI, the most gentle activation technique used in this paper, also for gp31 the amount of charge loss decreases.

The major differences between the two complexes using these experiments pertain to the effects of charge loss during activation/dissociation. We hypothesize that this loss is related to the structure of the ejected monomer, which is likely to be partially unfolded. The different structure and charging of the parents cause different dissociation pathways to become activated for the two protein complexes, resulting in different divisions of the charge over the fragment hexamers and ejected monomers and the amount of charge loss.

Despite the fact that the denatured average charge state for gp31 monomers is 11+, while the maximum charge state of the monomers formed via dissociation is around 8+, it seems that the monomer cannot be loaded to higher charge states during dissociation. Not even for the slowest activation technique used in this paper (SORI-CAD), will the monomer be unfolded enough to accommodate the maximum number of charges. For GroES the same is applicable, although less pronounced.

The GroES monomer loading is also limited around 8 charges, while the hexamer charge still increases with increasing parent charge.

The lower parent charge states for GroES are the prime cause of the different behavior under the different activation techniques. The monomers will reach their maximum loading capacity only for the highest GroES parent charge state in the FTMS on-resonance CAD and SORI-CAD experiments. For the q-ToF CAD experiment, both the gp31 monomer and the GroES monomer have reached their maximum loading capacity.

7. Conclusion

In this study, gas-phase differences between two highly similar large non-covalent protein complexes were examined, in an effort to relate their functional in vivo differences to differences in gas-phase stability and/or structure. The experiments reveal that there is no significant difference between the gas-phase stability of the two proteins. From this we deduce that the difference in function of the two complexes in vivo does not depend on the inter subunit interaction strength. Comparison of the different activation techniques with respect to the effects on charge distribution over the fragments proves to be interesting. The maximum loading capacities of the ejected monomers are

obtained and the correlation is shown between the time frame of activation and the degree of unfolding of the ejected monomer.

The investigation into the dissociation pathways for the two protein complexes revealed differences with respect to charge distribution over the dissociation products and with respect to the extend of charge loss during dissociation. There are no differences for NS-CAD and small differences for q-ToF CAD, but differences between the two complexes become more apparent with the more gentle activation mechanisms, FTMS on-resonance CAD and FTMS SORI-CAD. These differences indicate that there are structural features of the two complexes that are significantly different and that control the dissociation pathway. The major discriminants of the dissociation pathway are the parent charge state and the ability of the unfolded monomer to take up charges.

Acknowledgements

We thank Esther van Duijn for kindly providing the protein samples. This research is part of the research programme of the "Stichting voor Fundamenteel Onderzoek der Materie (FOM)", which is financially supported by the "Nederlandse organisatie voor Wetenschappelijk Onderzoek (NWO)". This work is part of the FOM/ALW program "Physical Biology II" under project number 01FB12-1.

References

[1] J.A. Loo, Int. J. Mass Spectrom. 200 (2000) 175.
[2] A.J.R. Heck, R.H.H. van den Heuvel, Mass Spectrom. Rev. 23 (2004) 368.
[3] K. Benkestock, G. Sundqvist, P.O. Edlund, J. Roeraade, J. Mass Spectrom. 39 (2004) 1059.
[4] K.J. Lightwahl, B.L. Schwartz, R.D. Smith, J. Am. Chem. Soc. 116 (1994) 5271.
[5] A.A. Rostom, P. Fucini, D.R. Benjamin, R. Juenemann, K.H. Nierhaus, F.U. Hartl, C.M. Dobson, C.V. Robinson, Proc. Natl. Acad. Sci. U.S.A. 97 (2000) 5185.
[6] S. Zhang, C.K. Van Pelt, D.B. Wilson, Anal. Chem. 75 (2003) 3010.
[7] J. Laskin, J.H. Futrell, Mass Spectrom. Rev. 24 (2005) 135.
[8] J. Laskin, J.H. Futrell, Mass Spectrom. Rev. 22 (2003) 158.
[9] F.M. Fernandez, V.H. Wysocki, J.H. Futrell, J. Laskin, J. Am. Soc. Mass Spectrom. 17 (2006) 700.
[10] E. van Duijn, P.J. Bakkes, R.M.A. Heeren, R.H.H. van den Heuvell, H. van Heerikhuizen, S.M. van der Vies, A.J.R. Heck, Nat. Methods 2 (2005) 371.
[11] F. Sobott, C.V. Robinson, Curr. Opin. Struct. Biol. 12 (2002) 729.
[12] P.B. Sigler, Z.H. Xu, H.S. Rye, S.G. Burston, W.A. Fenton, A.L. Horwich, Annu. Rev. Biochem. 67 (1998) 581.
[13] R.J. Ellis, Curr. Biol. 11 (2001) R1038.
[14] W.A. Houry, D. Frishman, C. Eckerskorn, F. Lottspeich, F.U. Hartl, Nature 402 (1999) 147.
[15] Z. Lin, H.S. Rye, Crit. Rev. Biochem. Mol. Biol. 41 (2006) 211.
[16] E. Deuerling, B. Bukau, Crit. Rev. Biochem. Mol. Biol. 39 (2004) 261.
[17] Y.C. Tang, H.C. Chang, A. Roeben, D. Wischnewski, N. Wischnewski, M.J. Kerner, F.U. Hartl, M. Hayer-Hartl, Cell 125 (2006) 903.
[18] A. Richardson, S.J. Landry, C. Georgopoulos, Trends Biochem. Sci. 23 (1998) 138.
[19] A.L. Horwich, G.W. Farr, W.A. Fenton, Chem. Rev. 106 (2006) 1917.
[20] J.F. Hunt, S.M. van der Vies, L. Henry, J. Deisenhofer, Cell 90 (1997) 361.
[21] D.K. Clare, P.J. Bakkes, H. van Heerikhuizen, S.M. van der Vies, H.R. Saibil, J. Mol. Biol. 358 (2006) 905.
[22] P.J. Bakkes, B.W. Faber, H. van Heerikhuizen, S.M. van der Vies, Proc. Natl. Acad. Sci. U.S.A. 102 (2005) 8144.
[23] J.F. Hunt, A.J. Weaver, S.J. Landry, L. Gierasch, J. Deisenhofer, Nature 379 (1996) 37.
[24] R.H.H. van den Heuvel, A.J.R. Heck, Curr. Opin. Chem. Biol. 8 (2004) 519.
[25] A. Richardson, C. Georgopoulos, Genetics 152 (1999) 1449.
[26] S.M. van der Vies, Methods Mol. Biol.: Chaperonin Protocols 140 (2000) 51.
[27] E. Quaite-Randall, A. Joachimiak, Methods Mol. Biol.: Chaperonin Protocols 140 (2000) 29.
[28] P.A. Voziyan, M.T. Fisher, Protein Sci. 9 (2000) 2405.
[29] T.H. Mize, I. Taban, M. Duursma, M. Seynen, M. Konijnenburg, A. Vijftigschild, C.V. Doornik, G.V. Rooij, R.M.A. Heeren, Int. J. Mass Spectrom. 235 (2004) 243.
[30] I.V. Chernushevich, B.A. Thomson, Anal. Chem. 76 (2004) 1754.
[31] S.H. Guan, A.G. Marshall, Int. J. Mass Spectrom. Ion Process. 158 (1996) 5.
[32] A.J.R. Heck, P.J. Derrick, Eur. Mass Spectrom. 4 (1998) 181.
[33] A.J. Kleinnijenhuis, M.C. Duursma, E. Breukink, R.M.A. Heeren, A.J.R. Heck, Anal. Chem. 75 (2003) 3219.
[34] R.H.H. van den Heuvel, E. van Duijn, H. Mazon, S.A. Synowsky, K. Lorenzen, C. Versluis, S.J.J. Brouns, D. Langridge, J.V.D. Oost, J. Hoyes, A.J.R. Heck, Anal. Chem. 78 (2006) 7473.
[35] A.N. Krutchinsky, I.V. Chernushevich, V.L. Spicer, W. Ens, K.G. Standing, J. Am. Soc. Mass Spectrom. 9 (1998) 569.
[36] F. Sobott, H. Hernandez, M.G. McCammon, M.A. Tito, C.V. Robinson, Anal. Chem. 74 (2002) 1402.
[37] N. Tahallah, M. Pinkse, C.S. Maier, A.J.R. Heck, Rapid Commun. Mass Spectrom. 15 (2001) 596.
[38] J. Zondlo, K.E. Fisher, Z.L. Lin, K.R. Ducote, E. Eisenstein, Biochemistry 34 (1995) 10334.
[39] E. van Duijn, D.A. Simmons, R.H.H. van den Heuvel, P.J. Bakkes, H. van Heerikhuizen, R.M.A. Heeren, C.V. Robinson, S.M. van der Vies, A.J.R. Heck, J. Am. Chem. Soc. 128 (2006) 4694.
[40] F. Sobott, C.V. Robinson, Int. J. Mass Spectrom. 236 (2004) 25.
[41] F. Sobott, M.G. McCammon, C.V. Robinson, Int. J. Mass Spectrom. 230 (2003) 193.
[42] C. Versluis, A. van der Staaij, E. Stokvis, A.J.R. Heck, B. de Craene, J. Am. Soc. Mass Spectrom. 12 (2001) 329.
[43] J.C. Jurchen, E.R. Williams, J. Am. Chem. Soc. 125 (2003) 2817.
[44] J.C. Jurchen, D.E. Garcia, E.R. Williams, J. Am. Soc. Mass Spectrom. 15 (2004) 1408.
[45] M.W.H. Pinkse, C.S. Maier, J.I. Kim, B.H. Oh, A.J.R. Heck, J. Mass Spectrom. 38 (2003) 315.
[46] R.M.A. Heeren, K. Vekey, Rapid Commun. Mass Spectrom. 12 (1998) 1175.
[47] X.H. Guo, M.C. Duursma, P.G. Kistemaker, N.M.M. Nibbering, K. Vekey, L. Drahos, R.M.A. Heeren, J. Mass Spectrom. 38 (2003) 597.
[48] L. Drahos, R.M.A. Heeren, C. Collette, E. De Pauw, K. Vekey, J. Mass Spectrom. 34 (1999) 1373.
[49] R.B.J. Geels, S.M. van der Vies, A.J.R. Heck, R.M.A. Heeren, Anal. Chem. 78 (2006) 7191.